Resonantly excited high-density exciton gas studied via broadband THz spectroscopy

Rupert Huber, Robert A. Kaindl, Ben A. Schmid, and Daniel S. Chemla
Department of Physics, University of California at Berkeley, and Material Sciences Division, E.O. Lawrence Berkeley National Laboratory, Berkeley, California 94720, USA

We report the density-dependent crossover of a resonantly photoexcited exciton gas from insulating to conducting phases. Broadband terahertz spectroscopy gives direct access to the exciton binding energy via intra-excitonic 1s-2p transitions. A strong shift, broadening, and ultimately the disappearance of this resonance occurs with decreasing inter-particle distance. Densities of excitons and unbound electron-hole pairs are followed quantitatively using a model of the composite free-carrier and exciton terahertz conductivity. Comparison with near-infrared absorption changes illustrates a significantly enhanced energy shift and broadening of the intra-excitonic resonance.

PACS numbers: 78.47.+p, 73.20.Mf, 78.67.De

In a many-particle electron-hole (e-h) system, density-dependent interactions govern its nature as an insulating gas of excitons or a conductive plasma of unbound e-h pairs [1]. At sufficiently low densities and temperatures, Coulomb attraction leads to the formation of charge-neutral excitons. With increasing density, the pairs overlap while the binding energy shrinks. Ultimately, the relative motion of the charges delocalizes fully as bound states cease to exist, giving rise to metallic behavior. This scenario is thought to underlie the excitonic Mott transition in a semiconductor [2–4], a long-standing topic of debate. Recently, Kappei *et al.* reported near-infrared photoluminescence studies in this high-density regime [5]. Quasi two-dimensional (2D) excitons in quantum wells are particularly suitable for such studies due to large binding energies and sharp optical resonances [5–7].

Numerous studies have investigated the near-infrared excitonic resonances just below the semiconductor band edge, and their broadening, bleaching, and energy shift due to photoexcited e-h pairs [8–16]. Broadening occurs via collisional interactions [8]. The energy shift is more subtle: with increasing density, phase-space filling and screening induce both a renormalization of single-particle states (and thus the band gap) as well as a reduction of the exciton binding energy [9, 10]. These two contributions counteract and cancel exactly in the three-dimensional case, where no shift of the exciton line is observed [11]. In quasi-2D systems, a small "blue" or "red"-shift remains depending on the conditions [12–15]. Hence, it is difficult to determine the density dependence of the exciton binding energy from such measurements.

Near-infrared exciton absorption arises from creation of excitons, not from transitions within existing populations, and mostly probes a subset of excitons with vanishing center-of-mass momentum. Terahertz (THz) spectroscopy, in contrast, constitutes a fundamentally different approach to study many-particle states. Transitions between internal states of excitons occur in this spectral region, which constitutes a direct measure of exciton densities and binding energies [17–22]. A recent THz study investigated the transient conducting and insulating phases that occur upon formation and ionization of exctions [21]. Furthermore, THz radiation is equally sensitive to the ultrafast dynamics of many-body correlations of unbound e-h pairs [23]. Thus, the interplay between optically generated excitons and unbound e-h pairs becomes directly observable. Until now, however, THz studies investigated a dilute exciton gas, while density-dependent modifications of the pair correlations were not reported.

In this paper, we employ broadband THz spectroscopy to probe the internal $1s$-$2p$ transition of resonantly photogenerated excitons at high densities. This technique gives full access to the low-energy complex dielectric function of the dense exciton gas. We directly trace the shift and broadening of the THz exciton resonance while the system undergoes a density-dependent transition from an insulating to a conductive state. The THz response is reproduced by an analytical model that quantitatively determines the densities of excitons and unbound e-h pairs. Comparing the THz spectra with the near-infrared response, we find a significantly enhanced energy shift and broadening of the intra-excitonic resonance.

Our sample consists of a stack of ten undoped 14-nm wide GaAs wells separated by 10-nm-wide $Al_{0.3}Ga_{0.7}As$ barriers. All measurements are performed at low temperatures ($T = 6$ K). The near-infrared absorption spectrum, shown in Fig. 1(a), is dominated by the $1s$ heavy-hole (HH) exciton line at 1.540 eV. Its linewidth is 0.8 meV (full width at half maximum, FWHM), pointing to a high sample quality. With increasing energy the $2s$HH and the $1s$ light-hole exciton appear, followed by transitions into the band-to-band continuum.

Heavy-hole excitons are resonantly photoexcited via spectrally-shaped near-infrared pulses derived from a 250-kHz Ti:sapphire amplifier. In order to inject high exciton densities, the pump spectrum [dashed line, Fig.1(a)] is tailored to a width (3.5 meV FWHM) distinctly larger than the low-intensity absorption line. This allows for continued overlap as the line broadens at higher densities. Figure 1(b) shows transient absorption spectra for several densities, monitored via time-delayed near-infrared probe pulses transmitted through the sample. At elevated pump fluences, we observe broadening, bleaching, and a slight blue shift of the near-infrared $1s$ absorption line. These changes are explained by the joint effects of

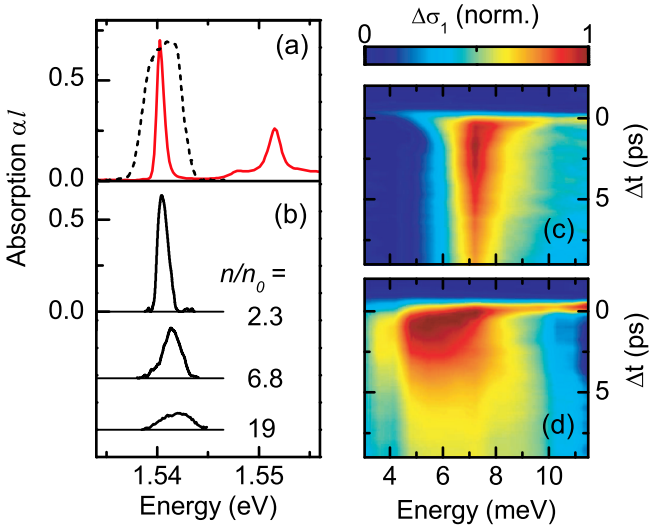

FIG. 1: (Color online). (a) Solid line: near-infrared, equilibrium absorption spectrum of the quantum well sample. Dashed curve: spectrum of the pump pulses. (b) Corresponding absorption spectra at delay time $\Delta t = 2.5$ ps after resonant $1s$HH excitation, for several densities n (where $n_0 \approx 1 \times 10^{10}\mathrm{cm}^{-2}$). The lattice temperature is $T_\mathrm{L} = 6$ K. (c,d) Ultrafast dynamics of the THz conductivity $\Delta\sigma_1(\omega)$ after resonant $1s$HH excitation for initial pair densities (c) $n \approx 2 \times 10^{10}\mathrm{cm}^{-2}$ and (d) $n \approx 14 \times 10^{10}\mathrm{cm}^{-2}$.

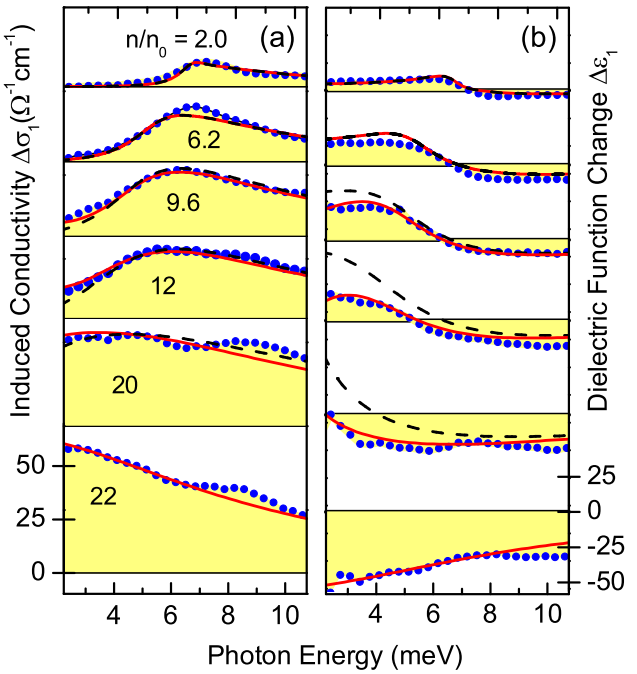

FIG. 2: (Color online). Photoinduced THz conductivity spectra $\Delta\sigma_1(\omega)$ [left panels] and dielectric function changes $\Delta\epsilon_1(\omega)$ [right panels] for various excited e-h pair densities n (given in units of $n_0 = 10^{10}\mathrm{cm}^{-2}$). Experimental data (solid dots) are measured at pump-probe delay $\Delta t = 2.5$ ps. Dashed lines: quasi-2D exciton model, solid lines: sum of exciton and Drude components, as explained in the text. At the two lowest densities, the free carriers vanish and the models coincide, while the model curve at the highest density shows a pure Drude response. Curves in each panel are shifted vertically for clarity, and are equally scaled.

phase-space filling and screening [9–15].

To probe the internal response of the bound e-h pairs, we employ broadband THz probe pulses generated by optical rectification. The real-time evolution of the THz electric field is detected by electro-optic sampling in a 500-μm-thick ZnTe crystal. We measure both the field transmitted through the sample in equilibrium, and its pump-induced change at a fixed pump-probe delay time Δt. From this, the complex optical conductivity $\tilde{\sigma}(\omega)$ and its transient change is obtained. The retrieval algorithm takes into account the multi-layer quantum well structure [21]. In the following, we will express the full THz dielectric response as $\tilde{\sigma}(\omega) = \sigma_1(\omega) + i\omega\epsilon_0[1 - \varepsilon_1(\omega)]$. The real part of the optical conductivity $\sigma_1(\omega)$ is a measure of the absorbed power density, while the real part of the dielectric function $\epsilon_1(\omega)$ provides a measure of the out-of-phase, inductive response.

Ultrafast transient changes in the THz conductivity $\Delta\sigma_1$ after near-infrared excitation are displayed in Figs. 1(c,d) as a function of the photon energy of the THz probe pulses and the pump-probe delay time Δt. These data, which are shown for two representative pump fluences, demonstrate a strong density dependence of the THz response. In the following, we will concentrate on features that emerge within the time resolution of our experiment of about 1 ps.

Figure 2 shows the THz response (solid dots) for various excitation densities n at delay time $\Delta t = 2.5$ ps. For the lowest density of $n = 2 \times 10^{10}$ cm^{-2}, a narrow asymmetric peak in $\Delta\sigma_1(\omega)$ at $\hbar\omega = 7$ meV demonstrates the existence of bound e-h pairs [21]. The maximum arises from the internal transition from $1s$ to $2p$ bound states, while the high-energy shoulder corresponds to transitions from $1s$ into higher bound and continuum states. The conductivity vanishes at low frequencies, which corroborates the insulating nature of this dilute exciton gas. The dispersive zero crossing of $\Delta\epsilon_1$ at a photon energy of 7 meV is characteristic of the well-defined intra-excitonic oscillator.

With increasing excitation density, three profound changes occur in the THz response as revealed in Fig. 2: (*i*) The area enclosed by the conductivity curve $\Delta\sigma_1(\omega)$ increases, while the near-infrared exciton line shown in Fig. 1(b) bleaches. Thus, with rising excitation density, oscillator strength is increasingly transferred from interband to intraband transitions. (*ii*) The width of the observed THz features strongly increases. (*iii*) Both the spectral maximum of $\Delta\sigma_1(\omega)$ and the zero crossing of $\Delta\epsilon_1(\omega)$ shift to lower frequencies. At the highest excitation density, the conductivity rises monotonically towards low frequencies and a zero crossing of the dielectric function is not observed. This behavior is indicative of a conducting phase in the absence of excitonic resonances.

For a quantitative analysis, we model the experimentally determined THz response (Fig. 2) via the low-energy dielectric function of two-dimensional excitons

$$\epsilon_{\rm X}(\omega) = \epsilon_\infty + \frac{n_{\rm X} e^2}{\epsilon_0 m} \sum_q \frac{f_{1s,q}}{(\omega_{1s,q}^2 - \omega^2) - i\omega\Gamma_{\rm X}} \qquad (1)$$

where ϵ_∞ and ϵ_0 are the background and vacuum dielectric constants, respectively, and e and m are the elementary charge and the reduced exciton mass. The oscillator strengths $f_{1s,q} = (2m\omega_{1s,q}/\hbar)|\langle\psi_{1s}|\mathbf{r}|\psi_q\rangle|^2$ for internal excitonic transitions from 1s to higher bound and unbound states are calculated using two-dimensional exciton wavefunctions ψ_i [2, 24]. We vary the exciton density $n_{\rm X}$, the energy position $E_{\rm 1s\to 2p} = \hbar\omega_{\rm 1s,2p}$, and the phenomenological exciton broadening parameter $\Gamma_{\rm X}$ to fit the measured conductivity curves. The results are shown as dashed curves in Fig. 2.

At low densities, good agreement with the experimental THz response is obtained. With increasing pump power, however, the model does not simultaneously reproduce both $\Delta\sigma_1$ and $\Delta\epsilon_1$. For parameters that optimally fit the measured conductivity (dashed lines in Fig. 2), the corresponding model $\Delta\epsilon_1$ deviates strongly from the experimental result. These problems can be resolved by considering additional low-frequency spectral weight, in the form of a coexisting plasma of unbound e-h pairs. The response of this two-component system is obtained by adding a Drude term to the dielectric function $\epsilon_{\rm X}$ of Eq. (1):

$$\epsilon(\omega) = \epsilon_{\rm X}(\omega) - \frac{n_{eh} e^2}{\epsilon_0 m} \frac{1}{\omega^2 + i\omega\Gamma_D} \qquad (2)$$

where n_{eh} is the density of unbound e-h pairs, and Γ_D is a phenomenological scattering rate. By including such unbound pairs, excellent agreement with the experiment is obtained even at high densities (solid curves in Fig. 2). The optimum values of the parameters are constrained by the different spectral response of excitons and unbound e-h pairs, and by the requirement to reproduce both functions, $\Delta\sigma_1(\omega)$ and $\Delta\epsilon_1(\omega)$, simultaneously and over a broad spectral range.

The resulting optimized fit parameters reveal details in the evolution of the complex many-body system with increasing density. Figure 3(a) shows the total density $n = n_{\rm X} + n_{eh}$ of excitons and unbound e-h pairs as a function of the pump power. Clearly, the pair density displays strong saturation at high pump powers as expected due to bleaching of the near infrared $1s$HH line. In the low-power limit the pair densities can also be estimated from the pump powers (linear near-infrared response). These values agree to within 50% with the densities n obtained from the THz model. In Fig. 3(b), we plot the density of unbound e-h pairs as a function of the total excited pair density n. At lower densities ($n < 5\times10^{10}$ cm^{-2}), only excitons are generated. With increasing n, the population share of unbound carriers becomes more significant. Beyond a critical density $\approx 2\times10^{11}$ cm^{-2}, an excitonic

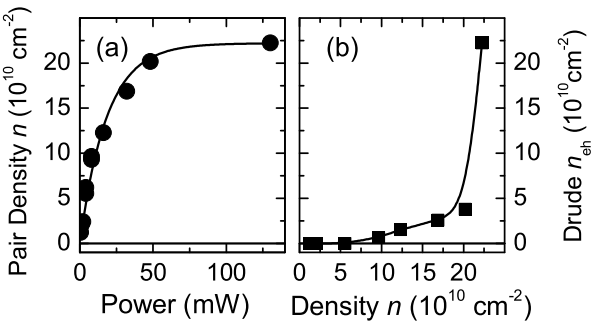

FIG. 3: Pair densities from the two-component model explained in the text. (a) Total excited pair density as a function of pump power. (b) Free carrier density as a function of the total pair density. Lines are a guide to the eye.

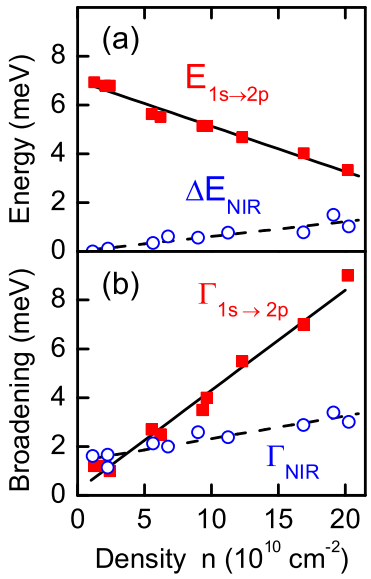

FIG. 4: (Color online). (a) Excitonic level spacing E_{1s-2p} (filled squares) measured via THz spectroscopy, and density-induced energy shift $\Delta E_{\rm NIR}$ (open circles) of the interband resonance. (b) Width Γ_{1s-2p} (filled squares) of the intra-excitonic $1s \to 2p$ resonance as fitted via the two-component model of Eq. 2, corresponding to the solid curves in Fig. 2. Open circles: width $\Gamma_{\rm NIR}$ (FWHM) of the near-infrared band edge absorption. Solid and dashed lines: linear fits to the data.

resonance is absent and the THz response can be fully explained by the Drude conductivity of unbound e-h pairs. This density compares well to values deduced recently from excitonic and interband photoluminescence spectra [5]. The THz response directly witnesses the transition from the insulating exciton gas to a conducting e-h plasma, and follows the changes of the excitonic fine structure.

A quantitative comparison of the near-infrared and THz response provides further insight into the high-density many-particle regime. Figure 4 illustrates the

changes in resonance energy and scattering rate involved in this transition. It shows (filled squares) the energy $E_{1s\rightarrow 2p}$ and width $\Gamma_{\rm X}$ of the THz exciton transitions. These curves reveal a striking red-shift and broadening that occurs in the $1s$-$2p$ intra-excitonic oscillator with increasing density. For comparison, the energy shift of the near-infrared $1s$HH resonance is also indicated [open circles, Fig. 4(a)]. The net shift is given by the counteracting effects of band gap renormalization and reduced exciton binding energy – its interpretation is thus elusive and requires model assumptions. In contrast, the intra-excitonic transitions observed here at THz frequencies are unaffected by bandgap shifts, and directly gauge the weakening of the binding energy.

From the near-infrared $1s$HH absorption band we evaluate the width $\Gamma_{\rm NIR}$ as a function of the excitation density [circles in Fig. 4(b)]. In addition to the spectrometer resolution, the finite optical thickness of the sample leads to a slight inhomogeneous broadening. The measured values of $\Gamma_{\rm NIR}$ are, however, a good upper bound for the width of the $1s$HH resonance. The density-dependence is well fitted by the relation $\Gamma_{\rm NIR}(n) = \Gamma_0 + \gamma_{\rm NIR} n$ [dashed line in Fig. 4(b)] with $\gamma_{\rm NIR} = 0.9 \times 10^{-11}{\rm meVcm}^2$, in quantitative agreement with literature values [8]. Remarkably, the density-dependent broadening of the THz response $\gamma_{\rm 1s\rightarrow 2p} = 4.1 \times 10^{-11}{\rm meVcm}^2$ (solid line) is about four times larger. We suggest that this results from enhanced sensitivity of the $2p$ exciton, not visible in near-infrared spectra, to screening and scattering: its radial extent (expectation value $\langle r_{2p}\rangle = 57.5\,{\rm nm}$ in our case) is six times that of $1s$ excitons. The combination of near-infrared and THz probes allows for a first direct analysis of this effect.

In conclusion, we report broadband THz studies of a high-density exciton gas resonantly photogenerated in GaAs/AlGaAs multiple quantum wells. With increasing excitation density, the far-infrared complex conductivity of this many-body system reveals a distinct red-shift of the intra-excitonic 1s-2p transition and a strong broadening of the 2p bound state, finally leading to the disappearance of the resonance. THz spectroscopy thus provides a direct gauge of bound and unbound pair densities, and enables the observation of the excitonic fine structure as it evolves under high-density conditions. We believe that this approach may prove valuable in future studies of high-density exciton physics including the low-temperature behavior of spatially-indirect pairs or interactions in lower dimensional structures.

We thank John Reno (Sandia National Laboratories) for providing quantum-well samples, and Nils Nielsen for interesting discussions. This work was supported by the Director, Office of Science, Basic Energy Sciences, U.S. Department of Energy, under contract DE-AC02-05CH11231. R. H. acknowledges support from the Alexander von Humboldt Foundation.

[1] E. I. Rashba, *Excitons* (North-Holland Publ. Co., Amsterdam, 1982).
[2] H. Haug and S. W. Koch, *Quantum theory of the Optical and Electronic Properties of Semiconductors* (World Scientific, Signapore, 2004).
[3] L. V. Keldysh and Y. V. Kopaev, Sov. Phys. Solid State **6**, 2219 (1965).
[4] N. F. Mott, Philos. Mag. **6**, 287 (1961).
[5] L. Kappei, J. Szczytko, F. Morier-Genoud, and B. Deveaud, Phys. Rev. Lett. **94**, 147403 (2005).
[6] J. Shah, *Ultrafast Spectroscopy of Semiconductors and Semiconductor Nanostructures* (Springer Verlag, 1999).
[7] D. S. Chemla and J. Shah, Nature **411**, 549 (2001).
[8] A. Honold, L. Schultheis, J. Kuhl, and C. W. Tu, Phys. Rev. B **40**, 6442 (1989).
[9] G. Tränkle, E. Lach, A. Forchel, F. Scholz, C. Ell, H. Haug, G. Weimann, G. Griffiths, H. Kroemer, and S. Subbanna, Phys. Rev. B **36**, 6712 (1987).
[10] M. Choi, K.-C. Je, S.-Y. Yim, and S.-H. Park, Phys. Rev. B **70**, 085309 (2004).
[11] G. W. Fehrenbach, W. Schäfer, J. Treusch, and R. G. Ulbrich, Phys. Rev. Lett. **49**, 1281 (1982).
[12] N. Peyghambarian, H. M. Gibbs, J. L. Jewell, A. Antonetti, A. Migus, D. Hulin, and A. Mysyrowicz, Phys. Rev. Lett. **53**, 2433 (1984).
[13] D. R. Wake, H. W. Yoon, J. P. Wolfe, and H. Morkoc, Phys. Rev. B **46**, 13452 (1992).
[14] G. Manzke, Q. Y. Peng, K. Henneberger, U. Neukirch, K. Hauke, K. Wundke, J. Gutowski, and D. Hommel, Phys. Rev. Lett. **80**, 4943 (1998).
[15] K. Litvinenko, D. Birkedahl, V. G. Lyssenko, and J. M. Hvam, Phys. Rev. B **59**, 10255 (1999).
[16] W. H. Knox, C. Hirlimann, D. A. B. Miller, J. Shah, D. S. Chemla, and C. V. Shank, Phys. Rev. Lett. **56**, 1191 (1986).
[17] T. Timusk, Phys. Rev. B **13**, 3511 (1976).
[18] R. H. M. Groeneveld and D. Grischkowsky, J. Opt. Soc. Am. B **11**, 2502 (1994).
[19] J. Černe, J. Kono, M. S. Sherwin, M. Sundaram, A. C. Gossard, and G. E. W. Bauer, Phys. Rev. Lett. **77**, 1131 (1996).
[20] M. Kira, W. Hoyer, T. Stroucken, and S. W. Koch, Phys. Rev. Lett. **87**, 176401 (2000).
[21] R. A. Kaindl, M. A. Carnahan, D. Hägele, R. Lövenich, and D. S. Chemla, Nature **423**, 734 (2003).
[22] I. Galbraith *et al.*, Phys. Rev. B **71**, 073302 (2005).
[23] R. Huber, F. Tauser, A. Brodschelm, M. Bichler, G. Abstreiter, and A. Leitenstorfer, Nature **414**, 286 (2001).
[24] R. A. Kaindl, D. Hägele, M. A. Carnahan, R. Lövenich, and D. S. Chemla (to be published).